Journal of Medicinal Chemistry

Article

pubs.acs.org/jmc

Effect of Phosphodiesterase 7 (PDE7) Inhibitors in Experimental Autoimmune Encephalomyelitis Mice. Discovery of a New Chemically Diverse Family of Compounds

Miriam Redondo,[†] José Brea,[‡] Daniel I. Perez,[†] Ignacio Soteras,[†] Cristina Val,[‡] Concepción Perez,[†] Jose A. Morales-García,[§,⊥] Sandra Alonso-Gil,[§,⊥] Nuria Paul-Fernandez,[∥,⊥] Rocío Martin-Alvarez,[∥,⊥] María Isabel Cadavid,[‡] María Isabel Loza,[‡] Ana Perez-Castillo,[§,⊥] Guadalupe Mengod,[∥,⊥] Nuria E. Campillo,[†] Ana Martinez,[†] and Carmen Gil*[,†]

[†]Instituto de Química Médica (CSIC), Juan de la Cierva 3, 28006, Madrid, Spain

[‡]Instituto de Farmacia Industrial, Facultad de Farmacia, Universidad de Santiago de Compostela, Campus Universitario Sur s/n, 15782 Santiago de Compostela, Spain

[§]Instituto de Investigaciones Biomédicas (CSIC-UAM), Arturo Duperier 4, 28029, Madrid, Spain

[∥]Instituto de Investigaciones Biomédicas de Barcelona (CSIC-IDIBAPS), Rosselló 161, 08036 Barcelona, Spain

[⊥]Centro de Investigación Biomédica en Red sobre Enfermedades Neurodegenerativas (CIBERNED), Spain

Supporting Information

ABSTRACT: Phosphodiesterase (PDE) 7 is involved in proinflammatory processes, being widely expressed both on lymphocytes and on certain brain regions. Specific inhibitors of PDE7 have been recently reported as potential new drugs for the treatment of neurological disorders because of their ability to increase intracellular levels of cAMP and thus to modulate the inflammatory process, as a neuroprotective well-established strategy. Multiple sclerosis is an unmet disease in which pathologies on the immune system, T-cells, and specific neural cells are involved simultaneously. Therefore, PDE7 inhibitors able to interfere with all these targets may represent an innovative therapy for this pathology. Here, we report a new chemically diverse family of heterocyclic PDE7 inhibitors, discovered and optimized by using molecular modeling studies, able to increase cAMP levels in cells, decrease inflammatory activation on primary neural cultures, and also attenuate the clinical symptoms in the experimental autoimmune encephalomyelitis (EAE) mouse model. These results led us to propose the use of PDE7 inhibitors as innovative therapeutic agents for the treatment of multiple sclerosis.

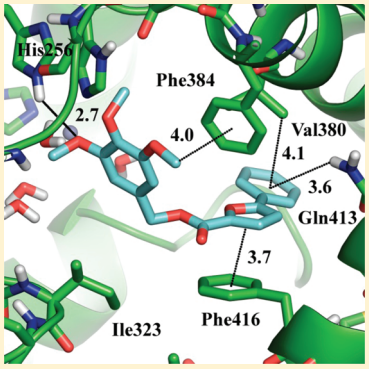

INTRODUCTION

The nucleotides cyclic adenosine 3′,5′-monophosphate (cAMP) and cyclic guanosine 3′,5′-monophosphate (cGMP) are two ubiquitous second messengers that mediate a variety of cellular responses. Two enzymatic processes control the intracellular levels of these nucleotides: the first one by regulation of their synthesis, achieved through the action of adenylate or guanylate cyclase, and the second one through their hydrolysis catalyzed by phosphodiesterases (PDEs).[1] Up to now there are 11 known families of PDEs that control the levels of cAMP and cGMP by catalyzing their hydrolysis to AMP and GMP, respectively. The family members are classified according to their sequence identity, cellular distribution, substrate specificity, and sensitivity to different PDE inhibitors,[2,3] being good targets for pharmacological intervention. In fact, one of the greatest advances in the PDE field in the past 15 years has been the increased availability and more recently the clinical use of family selective inhibitors.[4] Therefore, PDE inhibitors may have considerable therapeutic utility as anti-inflammatory agents, antiasthmatics, vasodilators, smooth muscle relaxants, cardiotonic agents, antidepressants, antithrombotics, and agents for improving memory and other cognitive functions.[5] The members of the PDE superfamily are well placed to be targets for pharmacological intervention. As elevation of intracellular cAMP level shows immunosuppressive and anti-inflammatory properties,[1,6] selective inhibitors of cAMP-specific PDEs have been widely studied as therapeutic agents for the treatment of human diseases.[5] The PDEs responsible for controlling specifically the intracellular levels of this nucleotide are PDE4, PDE7, and PDE8. More information is known about PDE4 being involved in the hydrolysis of cAMP within immune and central nervous system (CNS) cells. Thus, PDE4 inhibitors have been widely studied as efficient anti-inflammatory agents for different diseases.[7] However, a major drawback of these compounds is the significant emetic effects. To overcome these adverse effects, several strategies have been developed.[8] An alternative approach is to target different cAMP specific PDEs families, as PDE7[9] is also expressed in

Received: December 21, 2011
Published: March 5, 2012

 © 2012 American Chemical Society

T-cells and CNS and is a good target for the control of neuroinflammation.[10]

The PDE7 family is composed of two genes, PDE7A and PDE7B. High mRNA concentrations of both PDE7A and PDE7B are expressed in rat brain and in numerous peripheral tissues, although the distribution of these enzymes at the protein levels has not been reported. Within the brain PDE7A mRNA is abundant in the olfactory bulb, hippocampus, and several brain-stem nuclei.[11] The highest concentrations of PDE7B transcripts in the brain are found in the cerebellum, dentate gyrus of the hippocampus, and striatum.[12,13] There is very little information regarding the physiological functions regulated by PDE7. It has been shown that PDE7 is involved in proinflammatory processes and is necessary for the induction of T-cell proliferation.[14] Specific inhibitors of PDE7 have been recently reported as potential new drugs for the treatment of neurological disorders[15] by modulation of the inflammation process, a well-established neuroprotective strategy. Moreover, multiple sclerosis simultaneously involved pathologies on the immune system, T-cells, and specific neural cells, such as microglia and oligodendrocytes. Current pharmacological treatments for multiple sclerosis have severe drawbacks such as lack of efficacy and pharmacokinetics properties. PDE7 inhibitors may represent a well targeted and innovative therapy for this pathology.

Several years ago, our research group was the first to report the first PDE7 selective inhibitors.[16] Since then, a lot of effort has been made to increase potency and selectivity of these compounds, providing a great variety of diverse chemical compounds with interesting pharmacological profiles.[17]

Following our ongoing research on this field, we have recently demonstrated that PDE7 inhibitors belonging to the quinazoline family enhance neuroprotection and decrease neuroinflammation in well-characterized cellular and animal models of Parkinson's disease,[18] spinal cord injury,[19] and stroke.[20]

With the aim to design potent and specific PDE7 inhibitors, we developed a pharmacophore model for PDE7A1 inhibitors using Catalyst/Hypogen program to identify the chemical features that are responsible for the inhibitory activity.[21] Four pharmacophore features, such as one hydrogen bond acceptor, one aromatic ring, and two hydrophobic aliphatic points, were identified to be involved in inhibitor−PDE7 interaction (Chart 1).

Chart 1. Pharmacophore Features and Their Angle and Distance (Å) Relations

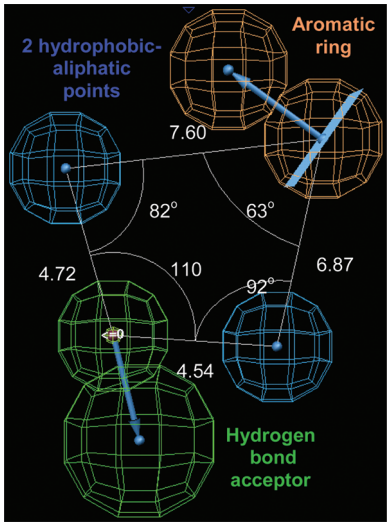

This pharmacophore model was able to predict the activity of an external test set of PDE7 inhibitors with a correlation coefficient of 0.96. New leads identification was carried out by performing virtual screening using validated pharmacophoric queries and four chemical databases (Maybridge, Chemical Diversity, Specs, and National Cancer Institute). Further data reduction was done employing virtual filters based on distances (T = 1.5 Å), angles (10°), and Lipinski's rules of five. According to this procedure, three new hits (**1**−**3**) were found as potential PDE7A1 inhibitors structurally diverse from those previously known[22] (Table 1). Then the biological activity of the hits was calculated using the catalytic domain of PDE7A1 and a radiometric assay.

Table 1. PDE7A1 Activities for Derivatives 1−3

Compound	Chemical structure	Experimental IC_{50} PDE7A1 (μM)
1	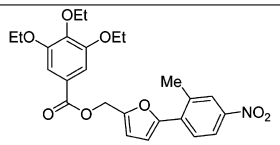	0.58±0.09[22]
2	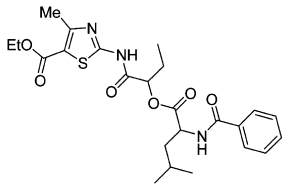	0.86±0.04[22]
3	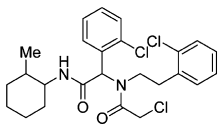	0.88±0.16[22]

These three hits were selected for further medicinal chemistry programs aimed to increase not only efficacy but also the ADME profile to be considered for further drug development in the neurodegenerative field. Here, the results obtained in the development of the family derived from the furan **1** and its therapeutic potential for multiple sclerosis are reported.

RESULTS AND DISCUSSION

Chemistry. The 5-(2-methyl-4-nitrophenyl)-2-furylmethyl 3,4,5-triethoxybenzoate (**1**) has a furan heterocycle between two substituted phenyl rings moieties. In particular, the structural modifications proposed are based on the modification of the number and nature of substituents attached to both phenyl rings and the variation of the linker between the furan and the alkyloxyphenyl ring (Chart 2).

The synthetic routes for the preparation of the furan derivatives are summarized in Schemes 1 and 2. The 5-phenyl-2-furylmethyl benzoate derivatives (Scheme 1) were obtained in one synthetic step after the coupling reaction of the alkyloxybenzoic acid and the corresponding 5-phenyl-2-furylmethanol. These furan alcohols were commercially available with the only exception being 5-(2,4-dichlorophenyl)-2-furylmethanol (**4**), which was synthesized by reduction of the 5-(2,4-dichlorophenyl)-2-furoic acid with lithium aluminum hydride as described in the Supporting Information.

dx.doi.org/10.1021/jm201720d | J. Med. Chem. 2012, 55, 3274−3284

Chart 2. Selected Lead Compound 1 for Further Optimization and Areas Where Modifications Have Been Done

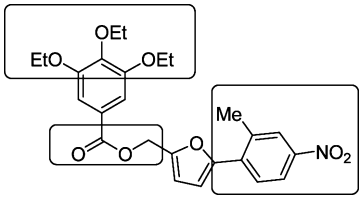

Scheme 1[a]

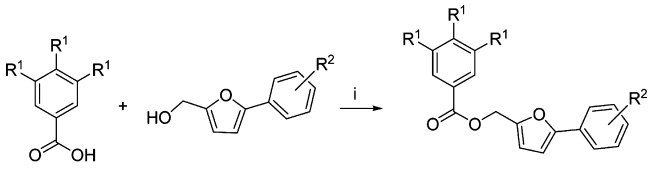

R^1 = OMe	R^2 = 2,4-diCl	5
	R^2 = 4-NO_2	6
R^1 = OEt	R^2 = H	7
	R^2 = 2,4-diCl	8
	R^2 = 4-NO_2	9
	R^2 = 4-Me	10

[a]Reagents: (i) coupling reagent, TEA, rt, CH_2Cl_2.

The synthesis of benzyl 5-phenylfuroate and benzyl-5-phenylfuramide derivatives (Scheme 2) involved the coupling of alkyloxybenzyl alcohol or alkyloxybenzylamine with the furoic acid derivative. Among different coupling reagents previously used, benzotriazol-1-yloxytripyrrolidinophosphonium hexafluorophosphate (PyBOP) was chosen as the most convenient one.

The structures of all the synthesized products were unequivocally confirmed by mass spectrometry, elemental analysis, and ^1H and ^{13}C NMR spectroscopic data.

In Vitro Evaluation of PDE7 Inhibition. The new derivatives here synthetized (**5**–**32**) were tested for their inhibitory potencies against PDE7A1 using recombinant human isoenzyme as described in the Experimental Section. All the compounds were tested at a fixed concentration (10 μM), performed in duplicate. The percentage of inhibition obtained on PDE7A1 for all the compounds at this concentration is shown in Table 2. From these data we can conclude that several new compounds are inhibitors of PDE7A1.

As the biological assay conditions differ from those previously used,[22] the lead compound **1** was also here evaluated to compare the data with the new synthesized derivatives. Noteworthy is the fact that when the lead compound **1** was evaluated in the new experimental conditions using the complete enzyme instead of the catalytic domain of PDE7A1, only 29% of PDE7A1 inhibition at 10 μM was found. Regarding these new data, modifications performed on the chemical structure of **1** increase in general the inhibition of PDE7A1.

When the percentage of PDE7A1 inhibition was greater than 50%, the dose–response curve was determined and the IC_{50} values were calculated (Table 3). Some of these new compounds present IC_{50} values for PDE7A1 inhibition in the low micromolar range, being suitable candidates to be further explored. A kinetic study varying cAMP concentration was performed with two of these compounds (**13** and **31**) to better characterize the enzymatic inhibition. Double-reciprocal plotting of the data is depicted in Figure 1. The intercept of the plot in the horizontal axis (1/[cAMP]) changes when the **13** and **31** concentrations increase, whereas the intercept in the vertical axis ($1/V$) does not change. These results suggest that furan derivatives act as competitive inhibitors of the cAMP binding site and allow us to determine the K_i of these inhibitors (5.91 and 7.22) for compounds **13** and **31**, respectively.

Scheme 2[a]

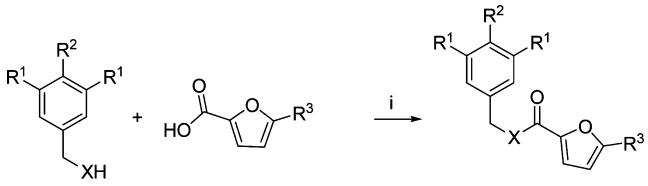

X=O, R^1=R^2 = OMe	R^3 = H	11
	R^3 = Me	12
	R^3 = Ph	13
	R^3 = 2-CF_3-Ph	14
	R^3 = 2-Cl-Ph	15
	R^3 = 2,4-diCl-Ph	16
	R^3 = 2-Cl, 5-CF_3-Ph	17
	R^3 = 2-NO_2, 4-Me-Ph	18
	R^3 = 2-NO_2, 4-Cl-Ph	19
	R^3 = 3-CF_3-Ph	20
	R^3 = 4-NO_2-Ph	21
	R^3 = 4-OMe-Ph	22
	R^3 = 4-Me-Ph	23
X=O, R^1=R^2 = OEt	R^3 = Ph	24
	R^3 = 2,4-diCl-Ph	25
	R^3 = 4-NO_2-Ph	26
	R^3 = 4-Me-Ph	27
X=O, R^1 = H, R^2 = OMe	R^3 = Ph	28
	R^3 = 2-NO_2, 4-Cl-Ph	29
X=NH, R^1=R^2 = OMe	R^3 = 3-CF_3-Ph	30
	R^3 = 2-NO_2, 4-Me-Ph	31
	R^3 = 2-NO_2, 4-Cl-Ph	32

[a]Reagents: (i) PyBOP, TEA, rt, CH_2Cl_2.

Table 2. PDE7A1 Inhibition of Compounds (5–32)

compd	% inh PDE7A1 @ 10 μM	compd	% inh PDE7A1 @ 10 μM
5	24.4 ± 13.4	**19**	49.1 ± 9.5
6	49.5 ± 3.0	**20**	14.0 ± 1.1
7	48.8 ± 11.1	**21**	48.0 ± 7.7
8	3.7 ± 2.0	**22**	14.0 ± 7.8
9	39.9 ± 8.6	**23**	30.7 ± 14.8
10	16.4 ± 1.1	**24**	30.8 ± 0.5
11	10.0 ± 6.9	**25**	31.1 ± 8.7
12	−9.9 ± 1.5	**26**	29.2 ± 0.2
13	57.9 ± 0.1	**27**	28.0 ± 4.5
14	54.9 ± 3.6	**28**	44.8 ± 1.2
15	34.6 ± 2.3	**29**	41.6 ± 6.5
16	38.3 ± 7.8	**30**	23.5 ± 0.4
17	8.0 ± 0.1	**31**	70.5 ± 4.6
18	28.8 ± 0.2	**32**	−10.3 ± 0.6

dx.doi.org/10.1021/jm201720d | J. Med. Chem. 2012, 55, 3274–3284

Table 3. IC_{50} for PDE7A1 of Selected Compounds and BRL50481 as Standard Reference[a]

	6	7	13	14	19	21	31
PDE7A1 IC_{50} (μM)	33.37 ± 8.1	12.34 ± 3.22	5.17 ± 1.11	2.63 ± 0.92	7.31 ± 3.57	14.07 ± 2.9	3.20 ± 1.23

[a] IC_{50}(BRL50481) = 0.09 μM.

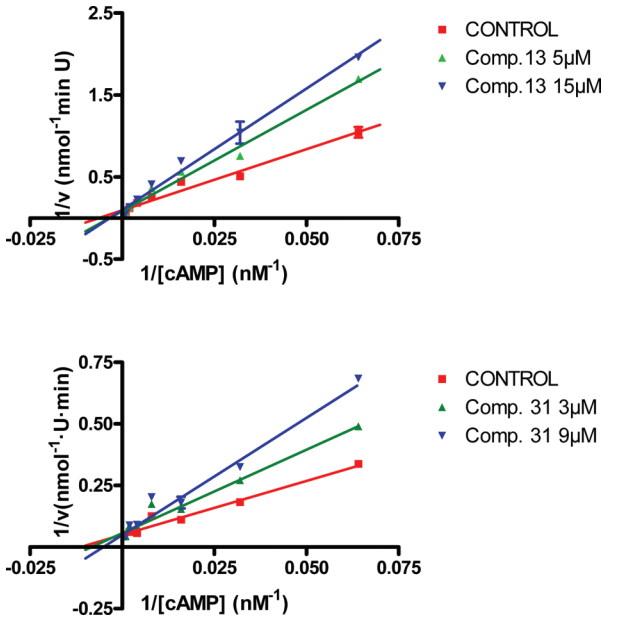

Figure 1. Studies of the PDE7A1 inhibition in the absence (control) and in the presence of two different concentrations of the furan derivatives **13** and **31** incubating different cAMP concentrations and measuring AMP formation. Data represent the mean ± SEM (vertical bars) of triplicate measurements.

Docking Studies. In order to gain some insight in the binding mode of our family of compounds, docking experiments were carried out with help from the Surflex method implemented in SYBYL according to the procedure described in the Experimental Section. Considering the kinetic studies results, the docking studies were focused on the cAMP binding site. After careful examination of docking solutions two binding modes that indicate the chemical structure−activity relationships (SARs) in this series of compounds were proposed. In fact, the different substituents and their location (ortho, meta, or para) when R^3 is a phenyl ring, determine which binding mode is selected.

The mainly binding mode (namely, "A" from now) is characterized by a hydrophobic interaction of the phenyl group in R^3 with Val380 and a NH−π interaction[23,24] with Gln413, which is in fact, a conserved residue among PDEs families.[25] A clear example of this binding mode is compound **13** (see Figure 2). In addition to these interactions, the furan moiety contributes to an increase in inhibition by means of a stacking interaction with another conserved residue as Phe416. Furthermore, the 3,4,5-trimethoxyphenyl ligand's moiety is located in a pocket where the ligand can benefit from a hydrogen bond between the methoxy group in R^2 and the proton H_ε of His256 group ($d_{H\varepsilon\cdots O}$ = 2.7 Å) and a hydrophobic interaction with Phe384.

When R^1 and R^2 are ethoxy groups (compound **24**), the binding mode remains mode "A" (see Figure 3). The presence of these bigger substituents forces the ligand to reorient the

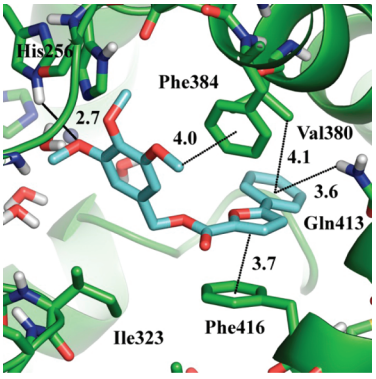

Figure 2. Proposed binding mode for compound **13** (PDB code 1ZKL) showing relevant interactions with nearby residues. Distances are given in angstroms.

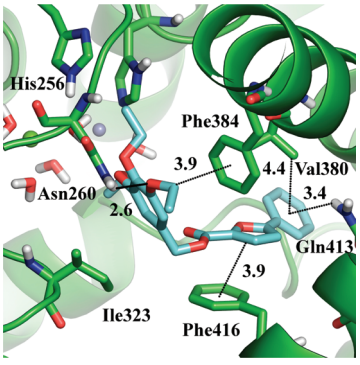

Figure 3. Proposed binding mode for compound **24** (for PDB code 1ZKL) showing relevant interactions with nearby residues. Distances are given in angstroms.

ester group, keeping a hydrophobic interaction with Phe384. This new location causes a weakening of the parallel stacking interaction between the furan ring and Phe416 (found for compound **13**) because of the displacement of the furan ring in order to keep the hydrophobic interaction between ligand's benzene ring in R_3 and Val380. As a result, compound **24** shows a lower percentage of PDE7A1 inhibition than compound **13** (Table 2).

Regarding the substituent located in the para position in the phenyl attached in R^3 such as a methyl group (compound **23**), the ligand orients this substituent facing it toward the Leu401 adopting thus the binding mode "B" (see Figure 4). This new orientation avoids potential steric clashes and allows the establishment of a new hydrophobic interaction between the methyl group and the side chain of Leu401. Meanwhile the previous stacking between the furan and Phe416 is mostly conserved. Furthermore, this new orientation forces the second phenyl ring to a new position where two new interactions with Ile323 are established which can help to stabilize the ligand in this new binding mode.

Finally, when the ester group linker is replaced by an amide one (compounds **30**−**32**), the conformation of the ligands

dx.doi.org/10.1021/jm201720d | J. Med. Chem. 2012, 55, 3274−3284

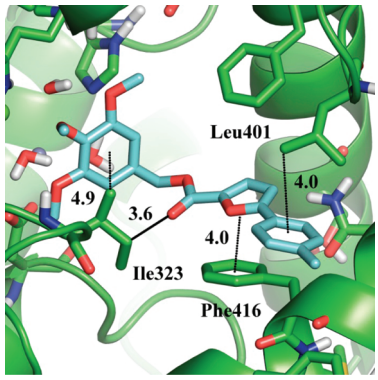

Figure 4. Proposed binding mode for compound **23** (PDB code 1ZKL) showing relevant interactions with nearby residues. Distances are given in angstroms.

dramatically changes by the formation of an intramolecular hydrogen bond between NH group and furan's oxygen. This conformation allows new stabilizing interactions between the phenyl ring with Leu401's side chain where it can interact hydrophobically (Figure 5).

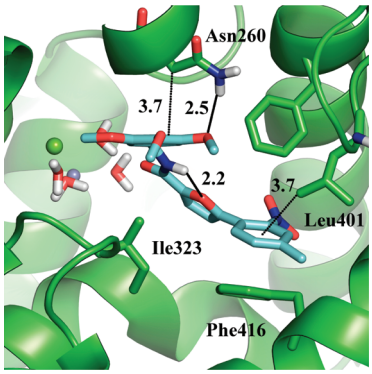

Figure 5. Proposed binding mode for compound **31** (PDB code 1ZKL) showing relevant interactions with nearby residues. Distances are in angstroms.

In Vitro Antiinflamatory Studies. Our next step was to explore whether these new PDE7 inhibitors are able to reduce the inflammatory response in different cell based assays. Thus, we used primary cultures of astrocytes and microglia treated with lipopolysaccharide (LPS), a potent inflammatory agent.

The potential anti-inflammatory activity of the selected PDE7 inhibitors (**7**, **13**, **14**, **19**, **21**, and **31**) was measured by evaluating the production of nitrites from primary cultured glial cells (astrocytes and microglia). To assess the safety of the compounds on cell culture, the astrocytes and microglia viability were checked using the 3-[4,5-dimethylthiazol-2-yl]-2,5-diphenyltetrazolium bromide (MTT) test at two different concentrations of the compounds. As both concentrations used do not affect the cell survival, they were selected for the antiinflammatory experiment.

Cultures were incubated with the indicated concentrations of compounds **7**, **13**, **14**, **19**, **21**, and **31** for 1 h, and then cells were treated for 24 h with LPS. When primary astrocytes and microglial cells were stimulated with LPS (Figures 6 and 7), a significant induction of nitrite production in the culture medium was produced, while if the PDE7 inhibitors were in the medium, a significant decrease of nitrite production was observed as a consequence of a reduction of the inflamatory cell response by the drug treatment. We used as standard references the well-known PDE4 inhibitor rolipram and the PDE7 inhibitor BRL50481.[26] These compounds showed a neuroprotective effect that was in accordance with our previously reported results,[20] confirming that these cell permeable PDE7 inhibitors are able to decrease neural inflammatory activation.

Candidate Selection for in Vivo Studies. The final aim of our study was to proof the potential efficacy of these new PDE7 inhibitors in a multiple sclerosis murine model. The selection of the candidate for in vivo studies was done based on pharmacological and pharmacokinetic properties.

Recently, potential cardiotoxic effect of long-term PDE3A inhibition was reported.[27] Thus, to avoid adverse effects in further development steps, we measured the inhibition on PDE3A of our selected compounds (Table 4).

Considering these new data, almost every derivative tested inhibit PDE3A at the same concentration that PDE7A1 was also inhibited, showing a lack of selectivity and opening safety concerns in further pharmacological development. However, derivative **13** shows an IC_{50} value 10-fold higher on PDE3A regarding PDE7A1 (ratio PDE7A1/PDE3A = 0.09), resulting in selection of this candidate for the next studies.

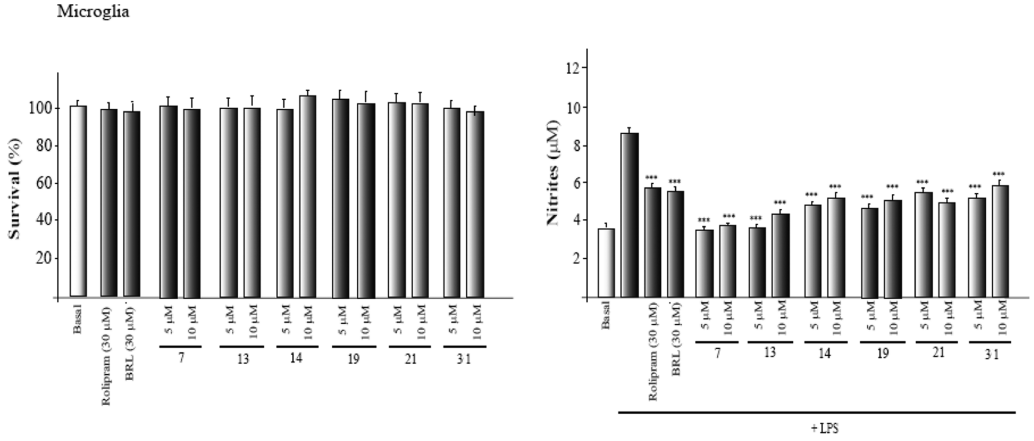

Figure 6. Cell viability and nitrite production. Glial cultures were treated during 16 h with rolipram (30 μM), BRL50481 (BRL, 30 μM), and compounds **7**, **13**, **14**, **19**, **21**, **31** (5 or 10 μM), and cell viability was measured. Some cultures were treated with lipopolysaccharide (LPS) in the presence or absence of compound at indicated concentrations, and the production of nitrites was measured as indicated in the Experimental Section. Values represent the mean ± SD of six replications in three different experiments: (***) $p < 0.001$ versus LPS-treated cells.

dx.doi.org/10.1021/jm201720d | J. Med. Chem. 2012, 55, 3274−3284

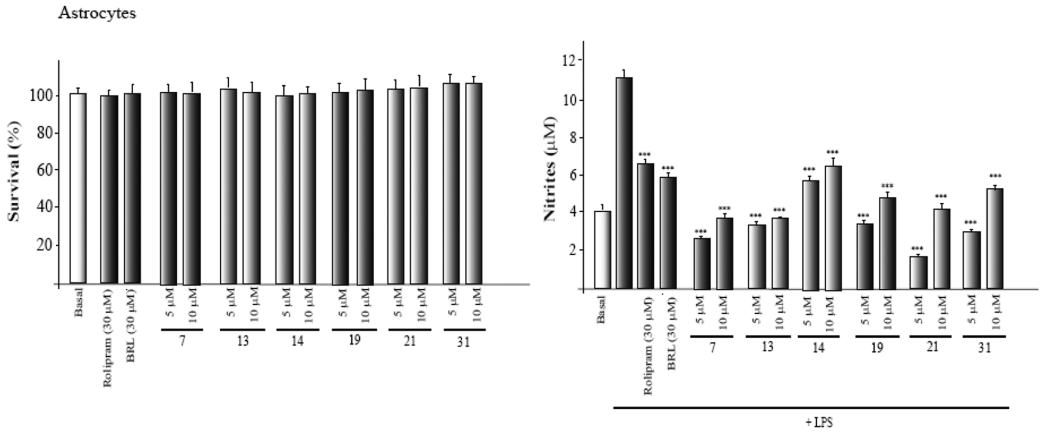

Figure 7. Cell viability and nitrite production. Astrocytes cultures were treated during 16 h with rolipram (30 μM), BRL50481 (BRL, 30 μM), and compounds **7**, **13**, **14**, **19**, **21**, **31** (5 or 10 μM), and cell viability was measured. Some cultures were treated with lipopolysaccharide (LPS) in the presence or absence of compound at indicated concentrations, and the production of nitrites was measured as indicated in the Experimental Section. Values represent the mean ± SD of six replications in three different experiments: (***) $p < 0.001$ versus LPS-treated cells.

Table 4. PDE3A Inhibition for Selected Compounds

compd	% inh PDE3A @ 10 μM	IC_{50}(PDE3A) (μM)	ratio PDE7A1/ PDE3A
7	3.0 ± 12.7	104.2 ± 36.6	0.12
13	46.1 ± 3.0	54.6 ± 12.1	0.09
14	74.9 ± 5.4	1.8 ± 0.85	1.44
19	11.0 ± 4	nd	nd
21	57.1 ± 12	3.4 ± 1.3	4.15
31	49.6 ± 1.2	3.9 ± 0.7	0.82

To evaluate isoenzyme specificity of **13**, inhibition of different cAMP isoenzymes was determined (Table 5). While marginal inhibition was found on PDE4B2, no activity was found on PDE7B and PDE4D3. The partial inhibition of PDE4B2 may increase the biological action of **13** in vivo because cAMP levels might be enhanced. Moreover, it is worth mentioning that inhibition of PDE4D3 is associated with the adverse emetic effects in the development of PDE4 inhibitors.[28] As derivative **13** does not inhibit this specific isoenzyme, its safety potential regarding PDEs inhibition is reinforced.

Table 5. IC_{50} (μM) on Different PDEs for Compound 13

compd	PDE7A1	PDE7B	PDE3A	PDE4B2	PDE4D3
13	5.1 ± 1.11	23.2 ± 4.4% @ 10 μM	54.6 ± 8.1	12.4 ± 4.2	66.3 ± 13.9

We also check the ability of derivative **13** to regulate intracellular cAMP levels in cell cultures. Two different compound concentrations (10 and 30 μM) were used, and in both cases we observed an increase of cAMP even more effective than the reported PDE7 inhibitor BRL50481[26] (Figure 8).

Finally, to decipher if this compound has the drug profile to be administered in vivo, we determined its ability to cross the blood–brain barrier (BBB), one of the major obstacles for the treatment of diseases in the central nervous system. The majority of compounds enter the brain by transcellular passive diffusion, which is driven by a concentration gradient between the blood and the brain.[29] Parallel artificial membrane permeability assay (PAMPA) is a high throughput technique developed to predict passive permeability through biological membranes. Here, we used the PAMPA-BBB method described by Di et al.,[30] employing a brain lipid porcine membrane to

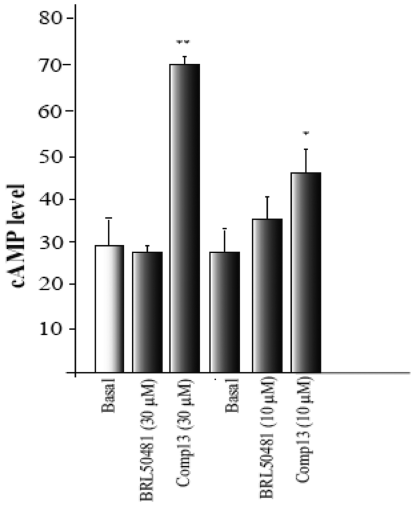

Figure 8. Intracellular cAMP level in raw cells treated with compound **13** at 30 and 10 μM.

determine the ability of compound **13** to penetrate into the brain. The in vitro permeabilities (P_e) of commercial drugs through lipid membrane extract together with compound **13** were determined and described. A good correlation between the experimental and described values, P_e(exp) = 1.1512 (bibl) − 0.8973 (R^2 = 0.9779), was obtained (see Supporting Information). From this equation, the P_e(exp) for **13** is (8.1 ± 0.1) × 10^{-6} cm s^{-1}. Following the pattern established in the literature for BBB permeation prediction[31] that classifies compounds as CNS+ when they present a permeability of >3.71 × 10^{-6} cm s^{-1}, we can consider that compound **13** is able to cross the BBB by passive permeation.

In Vivo Studies. Experimental Autoimmune Encephalomyelitis Model. The results found in cell cultures for the new PDE7 inhibitor **13** together with their ability to cross the BBB prompted us to evaluate it in chronic experimental autoimmune encephalomyelitis (EAE) mice, a well establish murine model for multiple sclerosis.

EAE was induced in C57BL/6J mice by immunization with MOG_{35-55} in complete Freund's adjuvant on day 0. Clinical signs and score were monitored up to day 41. Mice began to show neurological deficits on day 12, reaching a maximum

dx.doi.org/10.1021/jm201720d | J. Med. Chem. 2012, 55, 3274–3284

score around day 16. A therapeutic regimen of administration was chosen to test the PDE7 inhibitor in the EAE model. Thus, a daily intraperitoneal (i.p.) administration of compound **13** for 26 days started at day 5 after disease onset. The dose was selected considering the IC_{50} on the target and the cellular anti-inflammatory activity. As we can see in Figure 9A, a clear and significant attenuation of clinical symptoms during the first 16 days of treatment (day 32 after immunization) was observed. However, this behavior is lost in the last 10 days of treatment. The body weight curve (Figure 9B), reflects these findings, and the compound **13**-treated mice start to lose weight in the same timeframe as clinical scores decrease (described above).

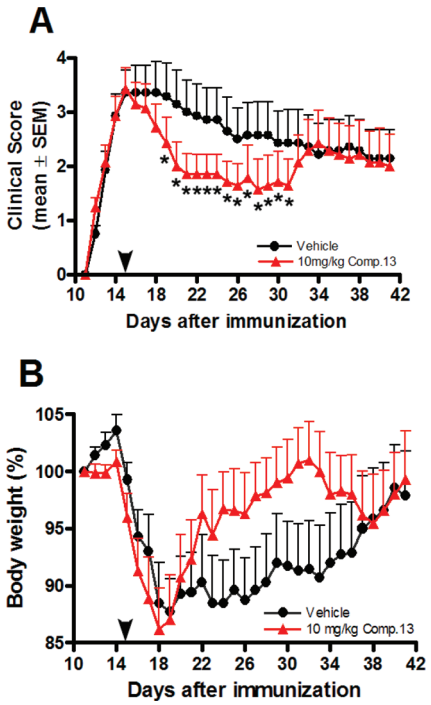

Figure 9. Therapeutic effect of compound **13** in MOG35-55-induced EAE in C57BL6J mice. Fourteen C57BL6J mice immunized with MOG35-55 at 100 μg/mouse in the presence of complete Freund's adjuvant developed clinical signs on day 12. Animals were divided into two groups. One group was treated with compound **13** starting from day 5 after the onset of the disease (arrowhead) for 26 days. Mice in the control group were administered vehicle only: (A) EAE scores in drug treatment; (B) percentage of body weight variation. Results were expressed as the mean ± standard error of the mean, and statistical differences in EAE scores between the vehicle and the treatment group were calculated by Mann–Whitney test (∗, $p < 0.0002$): (●) vehicle ($n = 7$); (▲) 10 mg/kg compound **13** ($n = 7$) i.p. daily.

This experiment showed for the first time efficacy of PDE inhibitors on a well established model of multiple sclerosis. Compound **13** administrated to the EAE when the worst neurological score was measured showed a recovery of the clinical symptoms reaching a statistically significant plateau of maximum effect from day 21 to 31 post immunization. However, this attenuation of the symptoms was counterbalanced by the worsening of the animals during the last 10 days of treatment until day 42, when the animals were sacrificed. To decipher if this effect is due to the administrated compound (stability, metabolism, etc.) or to the animal model, further studies are in progress.

CONCLUSIONS

PDE7 inhibitors represent a new class of innovative drugs with great potential for several neurological disorders. Their efficacy in animal models of Parkinson disease, stroke, and spinal cord injury has been recently reported, while their value for the treatment of multiple sclerosis is here disclosed. We presented the medicinal chemistry program around one hit found by using a pharmacophore model. The work led to a novel series of PDE7 inhibitors, chemically diverse from those known and containing a furan ring in their chemical structures.

The biological profile has been well characterized showing an increase of cAMP level and a reduction of the inflammatory response in primary neural cell cultures. Moreover, a clear strategy to select the best compound for in vivo testing, using pharmacodynamic and pharmacokinetic criteria, was followed. Finally, compound **13** was chosen because of its PDE7 selectivity and its ability to cross the BBB. This compound is able to reverse clinical symptoms in an EAE mice model. Together, these data supported the potential of PDE7 inhibitors for the therapeutic pharmacological treatment of multiple sclerosis.

EXPERIMENTAL SECTION

Chemical Procedures. Substrates were purchased from commercial sources and used without further purification. Melting points were determined with a Mettler Toledo MP70 apparatus. Flash column chromatography was carried out at medium pressure using silica gel (E. Merck, grade 60, particle size 0.040–0.063 mm, 230–240 mesh ASTM) with the indicated solvent as eluent. Compounds were detected with UV light (254 nm). ^{1}H NMR spectra were obtained on the Bruker AVANCE-300 spectrometer working at 300 MHz or on a Varian INOVA 400 spectrometer working at 400 MHz. Typical spectral parameters were as follows: spectral width 10 ppm, pulse width 9 μs (57°), data size 32 K. ^{13}C NMR experiments were carried out on a Bruker AVANCE-300 spectrometer operating at 75 MHz or on a Varian INOVA 400 spectrometer working at 100 MHz. The acquisition parameters were as follows: spectral width 16 kHz, acquisition time 0.99 s, pulse width 9 μs (57°), data size 32 K. Chemical shifts are reported in values (ppm) relative to internal Me_4Si, and J values are reported in Hz. Elemental analyses were performed by the Analytical Department at CENQUIOR (CSIC), and the results obtained were within ±0.4% of the theoretical values.

5-(4-Phenyl)-2-furylmethyl 3,4,5-Triethoxybenzoate (7). PyBOP (358 mg, 0.68 mmol) was added as coupling reagent to a solution of 3,4,5-triethoxybenzoic acid (175 mg, 0.68 mmol) with TEA (158 μL, 1.15 mmol) in CH_2Cl_2 (10 mL) followed by 5-phenyl-2-furylmethanol (100 mg, 0.57 mmol), and the resulting mixture was stirred at 25 °C during 12 h. The reaction mixture was evaporated in vacuo and the solid was purified by column chromatography on silica using hexane/ethyl acetate (8:1) as eluent to afford a yellow solid (246 mg, 87% yield), mp 71.1 °C. ^{1}H NMR (300 MHz, $CDCl_3$): δ 7.70–7.29, 6.64, 6.56, 5.33, 4.10, 1.42, 1.35. ^{13}C NMR (75 MHz, $CDCl_3$): δ 166.5, 153.0, 149.5, 149.1, 129.2, 125.7, 128.1, 125.7, 124.3, 124.4, 113.7, 108.8, 106.3, 69.4, 65.2, 59.2, 16.0, 15.2. MS (ES, $[M + K]^+$): m/z = 449. Anal. ($C_{25}H_{28}O_5$) C, H, O.

3,4,5-Trimethoxybenzyl 5-Phenyl-2-furoate (13). PyBOP (639 mg, 1.23 mmol) was added as coupling reagent to a solution of 5-phenyl-2-furoic acid (200 mg, 1.03 mmol) with TEA (284 μL, 2.06 mmol) in CH_2Cl_2 (10 mL) followed by 3,4,5-trimethoxybenzyl alcohol (210 μL, 1.27 mmol), and the resulting mixture was stirred at 25 °C during 23 h. The reaction mixture was evaporated in vacuo and the solid was purified by column chromatography on silica using hexane/ethyl acetate (8:1) as eluent to afford a white solid (90 mg, 24% yield), mp 98.4 °C. ^{1}H NMR (300 MHz, $CDCl_3$): δ 7.79, 7.45–7.26, 6.69, 5.29, 3.93–3.85. ^{13}C NMR (75 MHz, $CDCl_3$): δ 159.0, 158.2, 153.7, 143.9, 138.5, 131.7, 129.8, 129.4, 129.2, 125.3, 120.7, 107.3, 106.1, 67.1, 61.2, 56.6. MS (ES, $[M + Na]^+$): m/z = 391. Anal. ($C_{21}H_{20}O_6$) C, H, O.

dx.doi.org/10.1021/jm201720d | J. Med. Chem. 2012, 55, 3274–3284

3,4,5-Trimethoxybenzyl 5-(2-Trifluoromethylphenyl)-2-furoate (14). PyBOP (393 mg, 0.76 mmol) was added as coupling reagent to a solution of 5-(2-trifluoromethylphenyl)-2-furoic acid (200 mg, 0.76 mmol) with TEA (174 μL, 1.26 mmol) in CH_2Cl_2 (10 mL) followed by 3,4,5-trimethoxybenzyl alcohol (129 μL, 0.65 mmol), and the resulting mixture was stirred at 25 °C during 12 h. The reaction mixture was evaporated in vacuo and the solid was purified by column chromatography on silica using hexane/ethyl acetate (6:1) as eluent to afford a white solid (123 mg, 36% yield), mp 89.8 °C. ^{1}H NMR (300 MHz, $CDCl_3$): δ 7.80, 7.68, 7.53, 7.30, 6.79, 6.69, 5.30, 3.89, 3.86. ^{13}C NMR (75 MHz, $CDCl_3$): δ 158.8, 154.5, 153.7, 144.8, 138.5, 132.3, 131.6, 131.1, 129.5, 128.8, 127.3, 124.1, 120.2, 112.4, 106.1, 67.2, 61.3, 56.5. MS (ES, $[M + Na]^+$): m/z = 459. Anal. ($C_{22}H_{19}F_3O_6$) C, H, O.

3,4,5-Trimethoxybenzyl 5-(4-Chloro-2-nitrophenyl)-2-furoate (19). PyBOP (369 mg, 0.71 mmol) was added as coupling reagent to a solution of 5-(4-chloro-2-nitrophenyl)-2-furoic acid (200 mg, 0.71 mmol) with TEA (164 μL, 1.19 mmol) in CH_2Cl_2 (10 mL) followed by 3,4,5-trimethoxybenzyl alcohol (101 μL, 0.61 mmol), and the resulting mixture was stirred at 25 °C during 12 h. The reaction mixture was evaporated in vacuo and the solid was purified by column chromatography on silica using hexane/ethyl acetate (6:1) as eluent to afford a white solid (130 mg, 38% yield), mp 147.3 °C. ^{1}H NMR (300 MHz, $CDCl_3$): δ 8.37−7.87, 7.86, 7.30, 5.87, 4.48, 4.44. ^{13}C NMR (75 MHz, $CDCl_3$): δ 158.5, 153.8, 151.1, 148.4, 145.6, 138.5, 136.1, 132.8, 131.4, 131.2, 124.9, 122.0, 124.8, 120.2, 112.2, 106.0, 67.4, 61.3, 56.6. MS (ES, $[M + Na]^+$): m/z = 470. Anal. ($C_{25}H_{28}O_5$) C, H, O.

3,4,5-Trimethoxybenzyl 5-(4-Nitrophenyl)-2-furoate (21). PyBOP (509 mg, 0.98 mmol) was added as coupling reagent to a solution of 5-(4-nitrophenyl)-2-furoic acid (200 mg, 0.82 mmol) with TEA (227 μL, 1.64 mmol) in CH_2Cl_2 (10 mL) followed by 3,4,5-trimethoxybenzyl alcohol (168 μL, 0.98 mmol), and the resulting mixture was stirred at 25 °C during 24 h. The reaction mixture was evaporated in vacuo and the solid was purified by column chromatography on silica using hexane/ethyl acetate (4:1) as eluent to afford a white solid (34 mg, 10% yield), mp 161.2 °C. ^{1}H NMR (300 MHz, $CDCl_3$): δ 7.52, 7.93, 7.31, 6.95, 6.69, 5.30, 3.93−3.86. ^{13}C NMR (75 MHz, $CDCl_3$): δ 158.6, 155.4, 153.8, 147.9, 145.6, 143.2, 135.4, 131.4, 125.7, 124.8, 120.6, 110.5, 106.3, 67.5, 61.3, 56.6. MS (ES, $[M + Na]^+$): m/z = 436. Anal. ($C_{21}H_{19}NO_8$) C, H, N, O.

3,4,5-Trimethoxybenzyl-5-(4-methyl-2-nitrophenyl)-2-furamide (31). PyBOP (618 mg, 1.19 mmol) was added as coupling reagent to a solution of 5-(4-methyl-2-nitrophenyl)-2-furoic acid (300 mg, 1.19 mmol) with TEA (274 μL, 1.98 mmol) in CH_2Cl_2 (10 mL) followed by 3,4,5-trimethoxybenzylamine (173 μL, 0.99 mmol), and the resulting mixture was stirred at 25 °C during 12 h. The reaction mixture was evaporated in vacuo and the solid was purified by column chromatography on silica using hexane/ethyl acetate (3:1) as eluent to afford a yellow solid (56 mg, 14% yield), mp 114.2 °C. ^{1}H NMR (300 MHz, $CDCl_3$): δ 7.49, 7.34, 7.15, 6.65, 6.51, 4.48, 3.81, 3.75, 2.39. ^{13}C NMR (75 MHz, $CDCl_3$): δ 158.2, 153.9, 150.6, 148.4, 148.2, 141.1, 137.3, 133.9, 133.2, 125.2, 124.8, 120.7, 116.6, 111.5, 105.1, 61.3, 56.6, 43.8, 21.5. MS (ES, $[M + H]^+$): m/z = 427. Anal. $C_{22}H_{22}N_2O_7$ (C, H, N, O).

Radiometric Phosphodiesterase Inhibition Assay. The methodology used for measuring human recombinant PDE7A1, PDE7B, and PDE3A activity was based on a scintillation proximity assay (SPA) from Perkin-Elmer (TRKQ7090). The activity of the phosphodiesterase is measured by co-incubating the enzyme with $[^3H]$cAMP, and the hydrolysis of the nucleotide is quantified by radioactivity measurement after binding of $[^3H]$AMP to scintillation binding bead.

Either 0.02 unit of PDE7A1 (Calbiochem no. 524751), 0.02 unit of PDE3A (Calbiochem no. 524742), or 0.5 unit of PDE7B (Abcam no. ab79800) was incubated in a 96-well Flexiplate with 5 nCi $[^3H]$cAMP and inhibitors in 100 μL of assay buffer (contained in the kit) for 20 min at 30 °C. After the incubation time, an amount of 50 μL of a solution of SPA beads (approximately 1 mg per well) was added to each well and the plate was shaken for 1 h at room temperature. Finally, beads were settled for 30 min and radioactivity was detected in a Microbeta Trilux reader.

IC_{50} values were calculated by nonlinear regression fitting using GraphPad Prism. Data (radioactivity vs log concentration) were fitted to a sigmoidal dose−response equation: Y = Bottom + (Top − Bottom)/(1 + $10^{((\log IC_{50} - X)n)}$), where Bottom and Top were the minimum and maximal inhibition for PDE, respectively, IC_{50} was the concentration of compound that inhibited the PDE activity at 50%, and n was the slope of the concentration−response curve.

The mode of inhibitory action for compounds **13** and **31** was determined by varying the concentration of unlabeled cAMP in the reaction cocktail within the range of 5 nM to 2 μM in the presence of a fixed concentration of $[^3H]$cAMP tracer and inhibitor concentrations. Enzyme activity data were analyzed using Lineweaver−Burk plots using GraphPad Prism.

Fluorescence Polarization Phosphodiesterase Inhibition Assay. The ability of compounds to inhibit PDE4B2 (human recombinant) and PDE4D3 (human recombinant) was determined by IMAP fluorescence polarization (FP) assay (Molecular Devices R8175).

0.05 U of PDE4B2 (Calbiochem no. 524736) and PDE4D3 (Calbiochem no. 524733) were incubated in a 96-well black half-area plate with 1 nM fluorescein adenosine 3′,5′-cyclic phosphate (contained in the kit) and inhibitors in 40 μL of assay buffer. Plates were mixed on a shaker for 10 s and incubated at ambient temperature for 60 min. IMAP binding reagent was added (60 μL of a 1 in 600 dilution in binding buffer of the kit stock solution) to terminate the assay. Plates were allowed to stand at ambient temperature for 1 h. The FP ratio was measured with a Tecan Ultra Evolution reader.

IC_{50} values were calculated by nonlinear regression fitting using GraphPad Prism. Data (fluorescence polarization vs log concentration) was fitted to a sigmoidal dose−response equation: Y = Bottom + (Top − Bottom)/(1 + $10^{((\log IC_{50} - X)n)}$), where Bottom and Top were the minimum and maximal inhibition for PDE, respectively, IC_{50} was the concentration of compound that inhibited the PDE activity at 50%, and n was the slope of the concentration−response curve.

Molecular Modeling. To carry out docking analysis, chain A of protein structures was processed with help of SYBYL, version 8.0, software,[32] adding hydrogens and capping terminal residues with neutral ends. Then newly added hydrogen positions were optimized with MMFF94 force field until a 0.01 kcal/mol gradient was reached. Ligand geometries were also minimized with MMFF94 force field until a 0.01 kcal/mol gradient was reached.

The docking studies were performed with Surflex (SYBYL). An "Automatic" protocol was generated, and dockings were carried out using 20 initial conformations for each ligand allowing flexibility. Preminimization and postminimization were used by considering 100 solutions in each case. C_{score} scoring function was used with all four options, claiming a relaxed structure.

Visual inspection of solutions of selected ligands was carried out in order to find which ones allow the best agreement with SAR data. Finally the selected ligand−complex geometries were minimized with the MMFF94 force field until a 0.01 kcal/mol gradient was reached.

To test our docking protocol and validate the procedure, we carried out docking experiments for some selected 3D structures The first one was for the complex of 3,5-dimethyl-1-(3-nitrophenyl)-1*H*-pyrazole-4-carboxylic acid ethyl ester bound to PDE4D (PDB code 1Y2K), as this ligand shares a high similarity with some of our inhibitors. The high similarity between the docked solution (only one cluster within 2.0 Å rmsd of heavy atoms was found) and the experimental one gave us confidence in our protocol (rmsd of 0.2 Å of heavy atoms vs experimental results; see Figure S2 in the Supporting Information). In fact, the main difference between both orientations is related to the benzene with supports of a nitro group. This difference can be explained because of the lack of water W1016 from the PDB, which was not present in the model of PDE4D used for docking where only the metal coordination waters (W1003−W1008) were retained. On the other hand, in order to test our protocol specifically in PDE7, we carried out the docking experiment with the 3D structures of PDB codes 1ZKL and 3G3N. In the case of 1ZKL, the reproduction of the experimental binding mode of IBMX inhibitor was only possible (rmsd of 0.1 Å of heavy atoms vs experimental; see Figure S3 in the

Supporting Information) when waters W573 and W542 were added aside from the metal coordination waters (W504–W509). This fact is not surprising, as those two additional water molecules are within 3.0 Å from the ligand. As only those two structures of PDE7A were available at the moment of this study (PDB codes 1ZKL and 3G3N) and given the redocking results obtained for 3G3N, we decided to use structure 1ZKL for docking purposes. Finally, as the best redocking results were obtained for structure 1Y2K, which is the ligand that is the most similar to our inhibitors, we decided to retain only the metal coordination waters present in PDB code 1ZKL for docking.

Primary Cell Cultures. Glial cells were prepared from neonatal rat cerebral cortex, as previously described by Luna-Medina et al.[33] Briefly, after removal of the meninges the cerebral cortex was dissected, dissociated, and incubated with 0.25% trypsin/EDTA at 37 °C for 1 h. After centrifugation, the pellet was washed 3 times with HBSS (Gibco) and the cells were plated on noncoated flasks and maintained in HAMS/DMEM (1:1) medium containing 10% FBS. After 15 days the flasks were agitated on an orbital shaker for 4 h at 240 rpm at 37 °C. The supernatant was collected, centrifuged, and the cellular pellet containing the microglial cells was resuspended in complete medium (HAMS/DMEM (1:1) containing 10% FBS) and seeded on uncoated 96-well plates. Cells were allowed to adhere for 2 h, and the medium was removed to eliminate nonadherent oligodendrocytes. New fresh medium containing 10 ng/mL GM-CSF was added. The remaining astroglial cells adhered on the flasks were then trypsinized, collected, centrifuged, and plated onto 96-well plates with complete medium. The purity of cultures obtained by this procedure was >98% as determined by immunofluorescence with the OX42 (microglial marker) and the GFAP (astroglial marker) antibodies. After 1 week in culture, cells were treated with rolipram, BRL50481, and the different compounds (**7**, **13**, **14**, **19**, **21**, and **31**) at several concentrations. Cell viability was then measured after 16 h in culture. For nitrite release quantification some cultures were also treated with lipopolysaccharide (LPS, 10 μg/mL) alone or in combination with compounds.

Cell Viability Assay. Cell viability was measured using the MTT assay from Roche, based on the ability of viable cells to reduce yellow MTT to blue formazan. Briefly, cells cultured in 96-well plates and treated with the indicated compounds for 16 h were incubated with MTT (0.5 mg/mL, 4 h) and subsequently solubilized in 10% SDS/0.01 M HCl for 12 h in the dark. The extent of reduction of MTT was quantified by absorbance measurement at 595 nm according to the manufacturer's protocol.

Nitrites Measurement. Accumulation of nitrites in medium was assayed by the standard Griess reaction. After stimulation of cells with the different compounds, supernatants were collected and mixed with an equal volume of Griess reagent (Sigma). Samples were then incubated at room temperature for 15 min and absorbance read using a plate reader at 492/540 nm.

cAMP Measurements in Raw Cells. Quantification of cAMP was carried out using the EIA (enzyme immunoassay) kit from GE Healthcare. Briefly, raw cells were seeded at 3×10^4/well in 96-well dishes and incubated overnight before the assay. After 60 min of incubation with compound **13**, cAMP intracellular levels were determined following the manufacturer's instructions.

CNS Penetration: In Vitro Parallel Artificial Membrane Permeability Assay (PAMPA). Blood–Brain Barrier (BBB). Prediction of the brain penetration was evaluated using a parallel artificial membrane permeability assay (PAMPA).[30] Ten commercial drugs, phosphate buffer saline solution at pH 7.4 (PBS), ethanol, and dodecane were purchased from Sigma, Acros Organics, Merck, Aldrich, and Fluka. The porcine polar brain lipid (PBL) (catalog no. 141101) was from Avanti Polar Lipids. The donor plate was a 96-well filtrate plate (Multiscreen IP sterile plate PDVF membrane, pore size of 0.45 μm, catalog no. MAIPS4510) and the acceptor plate was an indented 96-well plate (Multiscreen, catalog no. MAMCS9610), both from Millipore. Filter PDVF membrane units (diameter 30 mm, pore size 0.45 μm) from Symta were used to filter the samples. A 96-well plate UV reader (Thermoscientific, Multiskan spectrum) was used for the UV measurements. Test compounds [(3–5 mg of caffeine, enoxacine, hydrocortisone, desipramine, ofloxacine, piroxicam, testosterone), 12 mg of promazine, and 25 mg of verapamile and atenolol] were dissolved in EtOH (1000 μL). Then 100 μL of this compound stock solution was taken and 1400 μL of EtOH and 3500 μL of PBS pH 7.4 buffer were added to reach 30% of EtOH concentration in the experiment. These solutions were filtered. The acceptor 96-well microplate was filled with 180 μL of PBS/EtOH (70/30). The donor 96-well plate was coated with 4 μL of porcine brain lipid in dodecane (20 mg mL^{-1}), and after 5 min, 180 μL of each compound solution was added. An amount of 1–2 mg of every compound, their ability to pass the brain barrier to be determined, was dissolved in 1500 μL of EtOH and 3500 μL of PBS, pH 7.4 buffer, filtered, and then added to the donor 96-well plate. Then the donor plate was carefully put on the acceptor plate to form a "sandwich", which was left undisturbed for 2 h and 30 min at 25 °C. During this time the compounds diffused from the donor plate through the brain lipid membrane into the acceptor plate. After incubation, the donor plate was removed. UV plate reader determined the concentration of compounds and commercial drugs in the acceptor and the donor wells. Every sample was analyzed at three to five wavelengths, in three wells, and in two independent runs. Results are given as the mean [standard deviation (SD)], and the average of the two runs is reported. Ten quality control compounds (previously mentioned) of known BBB permeability were included in each experiment to validate the analysis set.

EAE Induction and Treatment. Six-week-old female C57BL6 mice (15–20 g) were purchased from Harlan (Spain). All experimental procedures followed the European Communities Council Directive of November 24, 1986 (86/609/EEC). The protocol was approved by the Ethics Committee of the University of Barcelona and of the Generalitat de Catalunya. The mice were maintained on a 12 h light/dark cycle at a constant environmental temperature with free access to food and water for 1 week prior to experimentation.

EAE was induced by subcutaneous immunization with 100 μg of MOG_{35-55} peptide (EspiKem S.r.l., Italy) in 100 μL of complete Freund's adjuvant (CFA) (Sigma-Aldrich) enriched with *Mycobacterium tuberculosis* (H37Ra strain, Difco, Detroit, MI, U.S.). Mice were immediately intraperitoneally injected with 200 ng of *Bordetella pertussis* toxin (Sigma-Aldrich) and again 48 h after the immunization.

Animals (n = 13) were weighed and examined for clinical signs on a daily basis. Disease severity of EAE was graded according to a five-point scale: grade 0 = no disability; grad 1 = a flaccid tail; grade 2 = a mild but definite weakness of one or both hind legs; grade 3 = moderate paraparesis of one hind leg; grade 4 = no hind leg movement; grade 5 = a moribund state with little or no spontaneous movement and impaired respiration.[34]

Stock solution of the compound (100 mg/mL in DMSO) was diluted 1:50 in a solution of 5% Tocrisolve (Tocris, U.K.) in distilled water. Mice were treated through daily intraperitoneal (ip) injection starting on day 5 after the onset of the disease at a dose of 10 mg/kg of animal (n = 7) or with only vehicle (n = 7).

■ ASSOCIATED CONTENT

Ⓢ Supporting Information

Elemental analysis results of compounds **5**–**32**; experimental procedures for compounds **4**–**6**, **8**–**12**, **15**–**18**, **20**, **22**–**30**, and **32**; linear correlation between experimental and described values in the PAMPA-BBB assay; Figures S1 and S2. This material is available free of charge via the Internet at http://pubs.acs.org.

■ AUTHOR INFORMATION

Corresponding Author

*Phone: +34 91 5622900. Fax: +34 91 5644853. E-mail: cgil@iqm.csic.es.

Notes

The authors declare no competing financial interest.

■ ACKNOWLEDGMENTS

The authors gratefully acknowledge the financial support of Ministry of Science and Innovation (MICINN), Projects Nos. SAF2009-13015-C02-01, SAF2009-13015-C02-02, SAF2010-16365, SAF2009-1152, CTQ2009-07664, and PI10-01874; Instituto de Salud Carlos III (ISCiii), Project No. RD07/0060/0015 (RETICS program) and CIBERNED; Fundación Española para la Ciencia y la Tecnología (FECYT), Project No. FCT-09-INC-0367. M.R. and D.I.P. acknowledge pre- and postdoctoral fellowships from the CSIC (JAE program), respectively. BRAINco Biopharma is acknowledged.

■ ABBREVIATIONS USED

ADME, absorption, distribution, metabolism, and excretion; BBB, blood−brain barrier; cAMP, cyclic adenosine 3′,5′-monophosphate; CFA, complete Freund's adjuvant; cGMP, cyclic guanosine 3′,5′-monophosphate; CNS, central nervous system; DCC, *N*,*N*′-dicyclohexylcarbodiimide; DMEM, Dulbecco's modified Eagle's medium; DMSO, dimethyl sulfoxide; EAE, experimental autoimmune encephalomyelitis; EDTA, ethylenediaminetetraacetic acid; ES, electrospray; FBS, fetal bovine serum; FP, fluorescence polarization; GFAP, glial fibrillary acidic protein; GM-CSF, granulocyte-macrophage colony-stimulating factor; HAMS, Ham's F-12 nutrient mixture; HBSS, Hank's balanced salt solution; IC_{50}, inhibitory concentration 50; IMAP, immobilized metal ion affinity-based fluorescence polarization, MOG, myelin oligodendrocyte glycoprotein; mRNA, messenger ribonucleic acid; MS, mass spectrometry; MTT, 3-[4, 5-dimethylthiazol-2-yl]-2,5-diphenyltetrazolium bromide; NMR, nuclear magnetic resonance; LPS, lipopolysaccharide; PAMPA, parallel artificial membrane permeability assay; PBL, porcine polar brain lipid; PBS, phosphate buffer saline; PDE, phosphodiesterase; PDVF, polyvinylidene difluoride; PyBOP, benzotriazol-1-yloxytripyrrolidinophosphonium hexafluorophosphate; SAR, structure−activity relationship; SD, standard deviation; SDS, sodium dodecyl sulfate; SPA, scintillation proximity assay; TEA, triethylamine; THF, tetrahydrofuran; UV, ultraviolet light

■ REFERENCES

(1) Essayan, D. M. Cyclic nucleotide phosphodiesterase (PDE) inhibitors and immunomodulation. *Biochem. Pharmacol.* **1999**, *57*, 965−973.

(2) Conti, M.; Jin, S. L. The molecular biology of cyclic nucleotide phosphodiesterases. *Prog. Nucleic Acid Res. Mol. Biol.* **1999**, *63*, 1−38.

(3) Bender, A. T.; Beavo, J. A. Cyclic nucleotide phosphodiesterases: molecular regulation to clinical use. *Pharmacol. Rev.* **2006**, *58*, 488−520.

(4) Francis, S. H.; Conti, M.; Houslay, M. D. *Phosphodiesterases as Drug Targets*; Springer-Verlag: Berlin and Heidelberg, Germany, 2011.

(5) Lugnier, C. Cyclic nucleotide phosphodiesterase (PDE) superfamily: a new target for the development of specific therapeutic agents. *Pharmacol. Ther.* **2006**, *109*, 366−398.

(6) Allison, A. C. Immunosuppressive drugs: the first 50 years and a glance forward. *Immunopharmacology* **2000**, *47*, 63−83.

(7) Houslay, M. D.; Schafer, P.; Zhang, K. Y. Keynote review: phosphodiesterase-4 as a therapeutic target. *Drug Discovery Today* **2005**, *10*, 1503−1519.

(8) Giembycz, M. A. Life after PDE4: overcoming adverse events with dual-specificity phosphodiesterase inhibitors. *Curr. Opin. Pharmacol.* **2005**, *5*, 238−244.

(9) Conti, M.; Beavo, J. Biochemistry and physiology of cyclic nucleotide phosphodiesterases: essential components in cyclic nucleotide signaling. *Annu. Rev. Biochem.* **2007**, *76*, 481−511.

(10) Giembycz, M. A.; Smith, S. J. Phosphodiesterase 7A: a new therapeutic target for alleviating chronic inflammation? *Curr. Pharm. Des.* **2006**, *12*, 3207−3220.

(11) Miro, X.; Perez-Torres, S.; Palacios, J. M.; Puigdomenech, P.; Mengod, G. Differential distribution of cAMP-specific phosphodiesterase 7A mRNA in rat brain and peripheral organs. *Synapse* **2001**, *40*, 201−214.

(12) Sasaki, T.; Kotera, J.; Omori, K. Novel alternative splice variants of rat phosphodiesterase 7B showing unique tissue-specific expression and phosphorylation. *Biochem. J.* **2002**, *361*, 211−220.

(13) Reyes-Irisarri, E.; Perez-Torres, S.; Mengod, G. Neuronal expression of cAMP-specific phosphodiesterase 7B mRNA in the rat brain. *Neuroscience* **2005**, *132*, 1173−1185.

(14) Nakata, A.; Ogawa, K.; Sasaki, T.; Koyama, N.; Wada, K.; Kotera, J.; Kikkawa, H.; Omori, K.; Kaminuma, O. Potential role of phosphodiesterase 7 in human T cell function: comparative effects of two phosphodiesterase inhibitors. *Clin. Exp. Immunol.* **2002**, *128*, 460−466.

(15) Gil, C.; Campillo, N. E.; Perez, D. I.; Martinez, A. Phosphodiesterase 7 (PDE7) inhibitors as new drugs for neurological and inflammatory disorders. *Expert Opin. Ther. Pat.* **2008**, *18*, 1127−1139.

(16) Martinez, A.; Castro, A.; Gil, C.; Miralpeix, M.; Segarra, V.; Domenech, T.; Beleta, J.; Palacios, J. M.; Ryder, H.; Miro, X.; Bonet, C.; Casacuberta, J. M.; Azorin, F.; Piña, B.; Puigdomenech, P. Benzyl derivatives of 2,1,3-benzo- and benzothieno[3,2-*a*]thiadiazine 2,2-dioxides: first phosphodiesterase 7 inhibitors. *J. Med. Chem.* **2000**, *43*, 683−689.

(17) Castro, A.; Jerez, M. J.; Gil, C.; Martinez, A. Cyclic nucleotide phosphodiesterases and their role in immunomodulatory responses: advances in the development of specific phosphodiesterase inhibitors. *Med. Res. Rev.* **2005**, *25*, 229−244.

(18) Morales-Garcia, J.; Redondo, M.; Gil, C.; Alonso-Gil, S.; Martinez, A.; Santos, A.; Perez-Castillo, A. Phosphodiesterase 7 inhibition preserves dopaminergic neurons in cellular and rodent models of Parkinson disease. *PLoS One* **2011**, *6*, e17240.

(19) Paterniti, I.; Mazzon, E.; Gil, C.; Impllizzari, D.; Palomo, V.; Redondo, M.; Perez, D. I.; Esposito, E.; Martinez, A.; Cuzzocrea, S. PDE 7 inhibitors: new potential drugs for the therapy of spinal cord injury. *PLoS One* **2011**, *6*, e15937.

(20) Redondo, M.; Zarruk, J. G.; Ceballos, P.; Perez, D. I.; Perez, C.; Perez-Castillo, A.; Moro, M. A.; Brea, J.; Val, C.; Cadavid, M. I.; Loza, M. I.; Campillo, N. E.; Martinez, A.; Gil, C. Neuroprotective efficacy of quinazoline type phosphodiesterase 7 inhibitors in cellular cultures and experimental stroke model. *Eur. J. Med. Chem.* **2012**, *47*, 175−185.

(21) Jerez, M. J.; Castro, A.; Gil, C.; Martinez, A. Development of a pharmacophoric model for specific PDE7 inhibitors. *Drugs Future* **2004**, *29* (Suppl. A), 129.

(22) Gil, C.; Castro, A.; Jerez, M. J.; Ke, H.; Wang, H.; Ballester, S.; González-García, C.; Martínez, A. New PDE7 inhibitors leads for neurodegenerative diseases discovered by using a pharmacophoric model. *Drugs Future* **2008**, *33* (Suppl. A), 228.

(23) Vaupel, S.; Brutschy, B.; Tarakeshwar, P.; Kim, K. S. Characterization of weak NH−pi intermolecular interactions of ammonia with various substituted pi-systems. *J. Am. Chem. Soc.* **2006**, *128*, 5416−5426.

(24) Mohan, N.; Vijayalakshmi, K. P.; Koga, N.; Suresh, C. H. Comparison of aromatic NH···pi, OH···pi, and CH···pi interactions of alanine using MP2, CCSD, and DFT methods. *J. Comput. Chem.* **2010**, *31*, 2874−2882.

(25) Ke, H.; Wang, H. Crystal structures of phosphodiesterases and implications on substrate specificity and inhibitor selectivity. *Curr. Top. Med. Chem.* **2007**, *7*, 391−403.

(26) Smith, S. J.; Cieslinski, L. B.; Newton, R.; Donnelly, L. E.; Fenwick, P. S.; Nicholson, A. G.; Barnes, P. J.; Barnette, M. S.; Giembycz, M. A. Discovery of BRL 50481 [3-(*N*,*N*-dimethylsulfonamido)-4-methyl-nitrobenzene], a selective inhibitor of phosphodiesterase 7: in vitro studies in human monocytes, lung macrophages, and CD8+ T-lymphocytes. *Mol. Pharmacol.* **2004**, *66*, 1679−1689.

(27) Movsesian, M. A.; Kukreja, R. C. Phosphodiesterase inhibition in heart failure. *Handb. Exp. Pharmacol.* **2011**, 237−249.
(28) Robichaud, A.; Stamatiou, P. B.; Jin, S. L.; Lachance, N.; MacDonald, D.; Laliberte, F.; Liu, S.; Huang, Z.; Conti, M.; Chan, C. C. Deletion of phosphodiesterase 4D in mice shortens alpha(2)-adrenoceptor-mediated anesthesia, a behavioral correlate of emesis. *J. Clin. Invest.* **2002**, *110*, 1045−1052.
(29) Di, L.; Kerns, E. H.; Carter, G. T. Strategies to assess blood−brain barrier penetration. *Expert Opin. Drug Discovery* **2008**, *3*, 677−687.
(30) Di, L.; Kerns, E. H.; Fan, K.; McConnell, O. J.; Carter, G. T. High throughput artificial membrane permeability assay for blood-brain barrier. *Eur. J. Med. Chem.* **2003**, *38*, 223−232.
(31) Crivori, P.; Cruciani, G.; Carrupt, P. A.; Testa, B. Predicting blood−brain barrier permeation from three-dimensional molecular structure. *J. Med. Chem.* **2000**, *43*, 2204−2216.
(32) *SYBYL*, version 8.0; Tripos International (1699 South Hanley Road, St. Louis, MO, 63144, U.S.).
(33) Luna-Medina, R.; Cortes-Canteli, M.; Alonso, M.; Santos, A.; Martinez, A.; Perez-Castillo, A. Regulation of inflammatory response in neural cells in vitro by thiadiazolidinones derivatives through peroxisome proliferator-activated receptor gamma activation. *J. Biol. Chem.* **2005**, *280*, 21453−21462.
(34) McFarlin, D. E.; Blank, S. E.; Kibler, R. F. Recurrent experimental allergic encephalomyelitis in the Lewis rat. *J. Immunol.* **1974**, *113*, 712−715.